AGU PUBLICATIONS

Geophysical Research Letters

RESEARCH LETTER
10.1002/2014GL062767

Key Points:
- InSAR data reveal surface slip of 1–2 cm on multiple flexural-slip faults
- Surface slip was likely triggered by the 2013 *Mw* 6.6 Lake Grassmere earthquake
- Movement of flexural-slip faults may involve dynamic shaking due to earthquakes

Supporting Information:
- Figures S1–S5

Correspondence to:
Y. Kaneko,
y.kaneko@gns.cri.nz

Citation:
Kaneko, Y., I. J. Hamling, R. J. Van Dissen, M. Motagh, and S. V. Samsonov (2015), InSAR imaging of displacement on flexural-slip faults triggered by the 2013 *Mw* 6.6 Lake Grassmere earthquake, central New Zealand, *Geophys. Res. Lett.*, *42*, doi:10.1002/2014GL062767.

Received 4 DEC 2014
Accepted 16 JAN 2015
Accepted article online 24 JAN 2015

InSAR imaging of displacement on flexural-slip faults triggered by the 2013 *Mw* 6.6 Lake Grassmere earthquake, central New Zealand

Y. Kaneko[1], I. J. Hamling[1], R. J. Van Dissen[1], M. Motagh[2], and S. V. Samsonov[3]

[1]GNS Science, Lower Hutt, New Zealand, [2]GFZ German Research Centre for Geosciences, Potsdam, Germany, [3]Natural Resources Canada, Ottawa, Ontario, Canada

Abstract Interferometric Synthetic Aperture Radar (InSAR) data reveal surface slip on multiple faults triggered by the 2013 *Mw* 6.6 Lake Grassmere earthquake, New Zealand. Surface offsets of 1–2 cm occurred on previously inferred flexural-slip faults located ~4 km from the epicenter. We document dip slip on at least three different northeast striking, northwest dipping, flexural-slip faults located in the western limb of a syncline. The along-strike extent of the triggered slip is 1–1.5 km for each fault. Dislocation models suggest that triggered slip is confined to shallow depths (~800 m). Coulomb stress analysis indicates that slip was not triggered by the static stress change of the main shock but was likely caused by dynamic shaking during the passage of seismic waves. Our finding also provides an important clue on how some slip on shallow flexural-slip faults takes place.

1. Introduction

Understanding surface slip triggered by nearby earthquakes is important as triggered slip enhances our understanding of the exact locations of fault traces, fault interaction, and timescales over which some fault slip takes place. Surface slip, triggered by nearby large earthquakes, has been well documented in the Salton Trough region of southern California [e.g., *Williams et al.*, 1988; *Hudnut et al.*, 1989; *Rymer*, 2000; *Wei et al.*, 2011]. For example, using Interferometric Synthetic Aperture Radar (InSAR) data and field observations, *Wei et al.* [2011] found that slip of a few centimeters on numerous faults including the southern San Andreas fault was triggered by the 2010 *Mw* 7.2 El Mayor-Cucapah earthquake. However, susceptibility to triggering of surface slip in other tectonically active regions remains widely unknown.

In this work, we document and investigate surface slip on faults associated with the 16 August 2013 *Mw* 6.6 Lake Grassmere earthquake using Interferometric Synthetic Aperture Radar (InSAR) data. The Lake Grassmere earthquake occurred beneath the Clifford Bay region at the northeastern tip of the South Island of New Zealand, ~10 km east of Seddon (Figure 1). The earthquake was part of the 2013 Cook Strait earthquake sequence that began on 18 July 2013 (Figure 1) [*Holden et al.*, 2013]. The moment tensor solution and finite fault slip inversion for the Lake Grassmere earthquake suggest predominantly right-lateral slip with a hypocentral depth of ~8 km, rupture length of 25 km, and slip amplitude of up to 2.1 m, which did not reach the Earth's surface [*Hamling et al.*, 2014]. Using dislocation models, we estimate the depth extent and amplitude of the surface slip on previously inferred flexural-slip faults, which are bedding plane faults created by slip between the strata of synclines and anticlines [*Yeats*, 1986]. We analyze whether the surface slip on these inferred flexural-slip faults was more likely triggered by static stress transfer or by transient stresses generated by the passage of seismic waves.

2. InSAR Observations

We processed TerraSAR-X and RADARSAT-2 SAR data acquired over the Lake Grassmere area and formed two coseismic interferograms covering the 16 August Lake Grassmere earthquake (Figure 2). For TerraSAR-X, images were acquired in a descending pass on 3 and 25 August, with a radar incidence angle of ~24° and perpendicular baseline of 22 m (Figure 2a). For RADARSAT-2, images were acquired on 27 July and 20 August on a descending pass with a radar incidence angle of ~44° and perpendicular baseline of 27 m (Figure 2c). The TerraSAR-X data were processed using SARScape with topographic corrections made using a 3 arc sec (90 m) digital elevation model (DEM) generated by the NASA shuttle Radar Topography Mission

©2015. American Geophysical Union. All Rights Reserved.

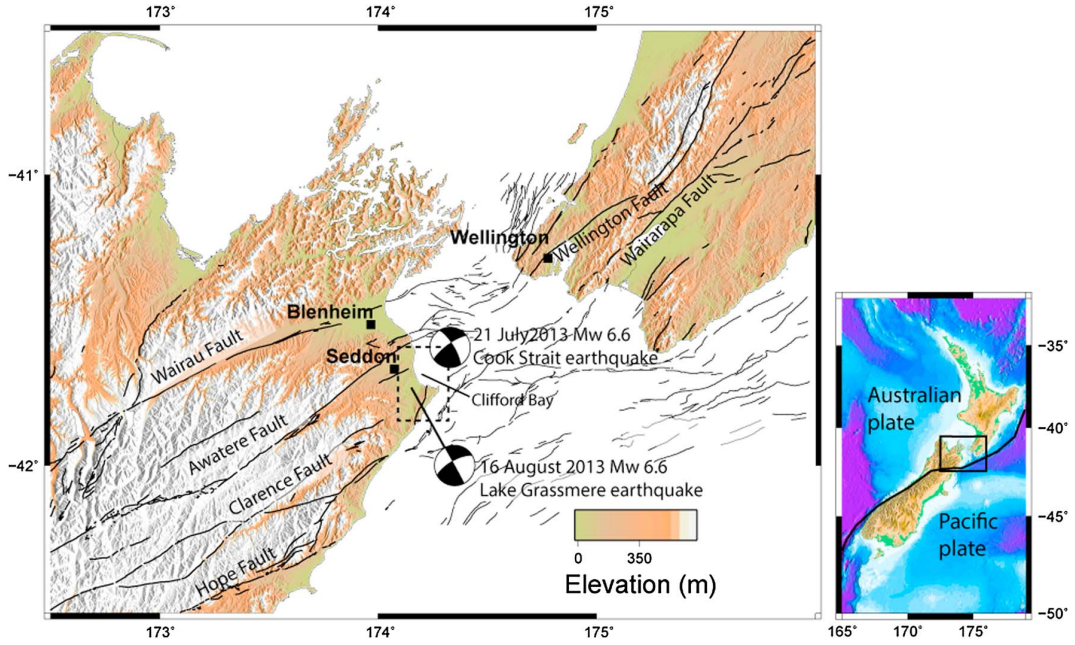

Figure 1. Map of central New Zealand with color-shaded topography and surface traces of active faults from New Zealand Active Fault Database [*Pondard and Barnes*, 2010; *Litchfield et al.*, 2014]. The dashed black rectangle shows our study area. Focal mechanisms of the 21 July 2013 Cook Strait and 16 August 2013 Lake Grassmere earthquakes are also indicated. The right inset shows the location of the plate boundary between the Pacific and Australian plates. The solid black rectangle corresponds to the region shown in the main figure. Tectonic motion in the region is transpressional resulting from the transition from oblique subduction in the North Island to strike-slip motion in the South Island [e.g., *Wallace et al.*, 2012].

[*Farr et al.*, 2007]. Processing of the RADARSAT-2 data was done using GAMMA [*Wegmüller and Werner*, 1997]. The topographic corrections were made using a 30 m ASTER DEM. Both interferograms were filtered via a power spectrum filter and were unwrapped using the minimum cost flow algorithm [*Costantini*, 1998].

While the coseismic interferograms are dominated by the long-wavelength signature of crustal deformation due to the *Mw* 6.6 Lake Grassmere earthquake, we found localized discontinuities in both wrapped and unwrapped phases, indicating the occurrence of surface slip (Figures 2b and 2c). The observed offsets do not correlate with local topography (Figure 2d). Coherence is poor in areas around Lake Grassmere due to liquefaction and numerous small-scale (meters to tens of meters) landslides [*Van Dissen et al.*, 2013]. The best measurements of the observed slip were obtained with 1.5 cm wavelength X band TerraSAR-X data, which were found to be less noisy (Figure 2b). Discontinuities in line-of-sight (LOS) displacement along three profiles shown in Figure 2 indicate surface slip on three parallel fault segments with strikes ranging from 205° to 215° and along-strike extents of 1–1.5 km for each segment. A fault-perpendicular distance between the most northwesterly fault and the most southeasterly fault that experienced surface slip is ~1 km.

The sites of the observed slip are located ~4 km away (to the southeast) from the surface projection of the 16 August Lake Grassmere event (dotted line in Figure 2a). Since the LOS displacement is essentially discontinuous across the fault traces (Figure 2d), the observed deformation is caused by localized fault slip and not by a response of compliant fault zones to static stress changes [*Fialko*, 2004]. The localized fault slip was likely triggered by the *Mw* 6.6 Lake Grassmere earthquake since the observed slip occurred sometime during the overlapping time period of the InSAR observations (see the time line in Figure 2). We do not attribute any of the observed slip to aftershocks as there were no reported shallow (< 8 km depth) aftershocks in this region during the time period of the InSAR observations (Figure S1 in the supporting information). Additionally, we did not find evidence of triggered surface slip in other areas.

The direction and amplitude of the inferred surface offsets can be estimated from the InSAR data. Only two offsets in LOS displacement are seen in the RADARSAT-2 interferogram due to lack of coherence and lower resolution (Figure 2d). All the estimated offsets were northwest side up. There are possibly other minor offsets in LOS displacement, but they are less clear. The largest offsets observed in Profile X–X′

©2015. American Geophysical Union. All Rights Reserved.

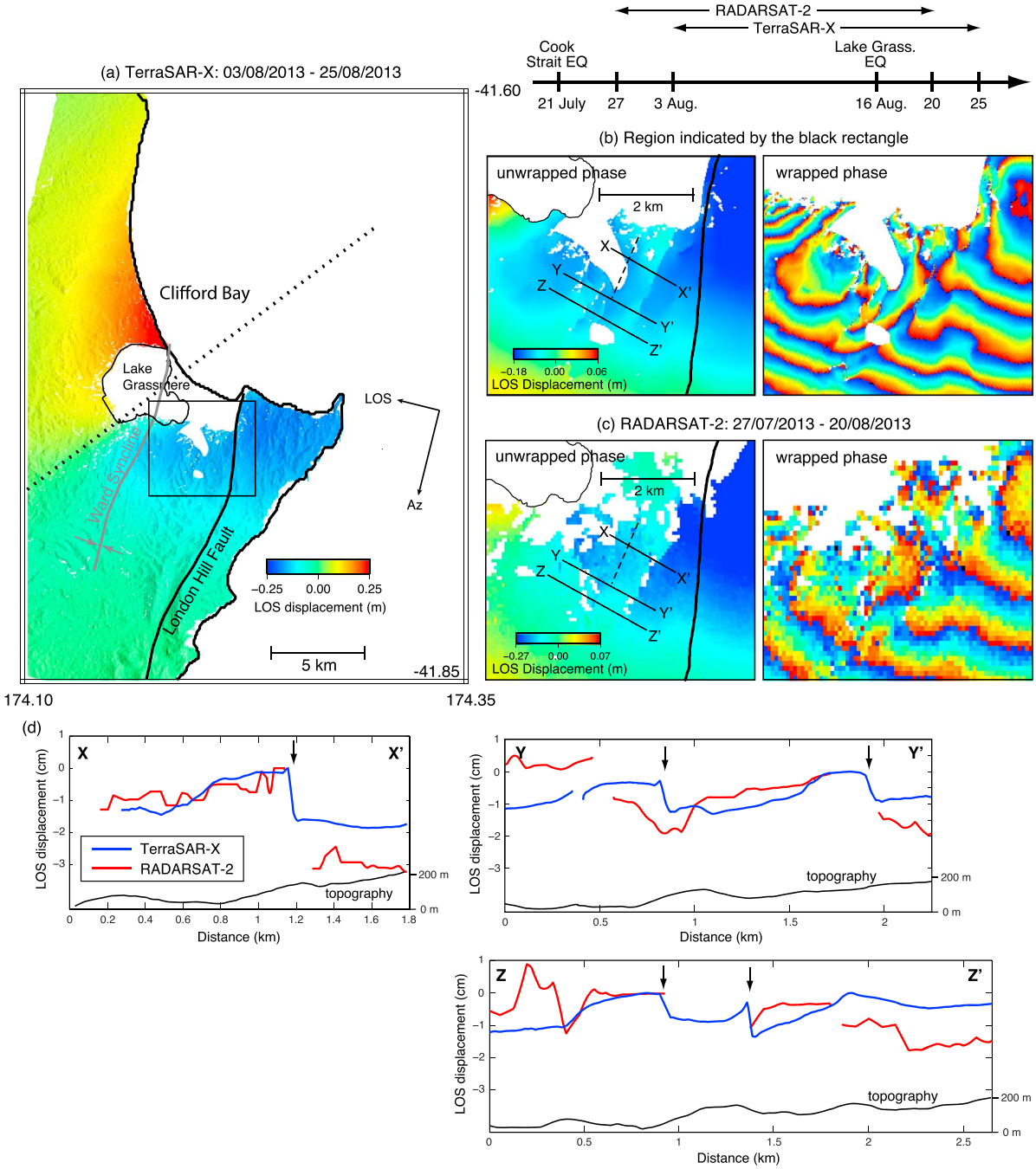

Figure 2. Line-of-sight (LOS) displacement of the Earth surface from (a) a TerraSAR-X interferogram, (b) a zoom-in view within the black rectangle for unwrapped and wrapped phases, and (c) RADARSAT-2 interferograms covering the same area. Arrows indicate the flight (Az) and LOS directions for TerraSAR-X. The flight direction is close (3° difference) to that for RADARSAT-2. A time line for radar acquisition dates is shown in the top. The dotted black line in Figure 2a corresponds to surface projection of a fault plane associated with the *Mw* 6.6 Lake Grassmere earthquake from *Hamling et al.* [2014]. The dashed black lines in Figures 2b and 2c correspond to the location of a known flexural-slip fault scarp [*Townsend and Little*, 1998]. (d) Profiles of the LOS displacement and topography from X to X′, Y to Y′, and Z to Z′. The LOS displacements are vertically shifted to roughly align with one another. Discontinuities in LOS displacement marked by the arrows correspond to the locations of surface slip.

©2015. American Geophysical Union. All Rights Reserved.

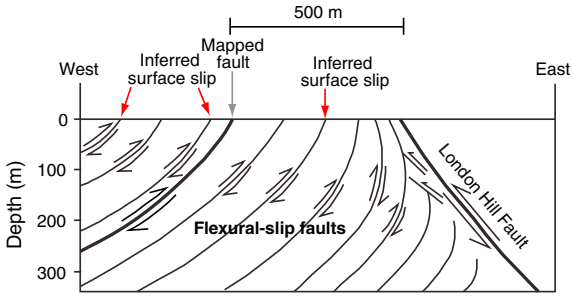

Figure 3. Sketch illustrating a cross-sectional view of faults in the study area. The sketch is constructed based on a geological cross section in this region [*Townsend and Little*, 1998, Figure 6]. Approximate locations of the inferred surface slip are indicated by the red arrows.

correspond to 1.7 and 2.0 cm for the TerraSAR-X and RADARSAT-2 interferograms, respectively (Figure 2d). Since the flight (Az) directions of both satellites are approximately parallel to the orientations of the inferred faults, the InSAR observations are insensitive to strike-slip motion of the faults. In this case, the horizontal (fault-perpendicular) and vertical ground offsets U_h and U_u can be expressed as

$$U_h \sin(\lambda_{Ter}) + U_u \cos(\lambda_{Ter}) = d_{Ter}$$
$$U_h \sin(\lambda_{Rad}) + U_u \cos(\lambda_{Rad}) = d_{Rad} \ ,$$

where λ_{Ter} and λ_{Rad} are the look angles for the TerraSAR-X and RADARSAT-2 satellites, respectively, and d_{Ter} and d_{Rad} are measured offsets in LOS displacement. For the largest offsets in profile X–X′ (Figure 2d), we obtain 1.8 and 1.1 cm for horizontal and vertical offsets, respectively, with a dip-slip amplitude of 2.1 cm. Note that the resolved horizontal and vertical offsets are not well constrained because of the similar look angles for these satellites. For example, ±0.2 cm uncertainties in estimated LOS offsets (d_{Ter} and d_{Rad}) lead to ±0.9 and ±0.6 cm in the horizontal and vertical offsets, respectively. If both ascending and descending modes of satellite data were available, the horizontal and vertical motion would be better resolved [e.g., *Wright et al.*, 2004].

The locations and strikes of faults associated with the observed surface slip do not coincide with those of mapped fault traces [*Rattenbury et al.*, 2000]; we suggest that slip likely occurred on previously inferred northwest dipping flexural-slip faults that dip toward the west in this region [*Townsend and Little*, 1998] (Figure 3). Additional support for this interpretation comes from the fact that a known scarp of a flexural-slip fault (dashed line in Figures 2b and 2c) runs parallel to the observed offsets. Furthermore, the direction of the slip estimated from the InSAR data is consistent with the expected sense of slip for flexural-slip faults, which are produced by bedding-parallel slip between the layers of the folded strata (Figure 3). The northeast striking, northwest dipping flexural-slip faults, which formed during the folding of the Ward syncline (Figure 2a), are thought to extend down to several hundred meters [*Townsend and Little*, 1998]. Stratigraphic columns west of the London Hill fault suggest that rock units in the area of flexural-slip faulting are Pliocene siltstones and sandstones that rest unconformably upon the Torlesse Terrane situated at a depth greater than 1 km [*Townsend and Little*, 1998]. Since the rock units across the flexural-slip faults are quite similar, the inferred offsets in LOS displacement were unlikely caused by differential settling of materials across the faults. We cannot rule out the possibility of oblique displacement on the inferred flexural-slip faults, although there is no evidence of strike-slip motions on the known scarp [*Townsend and Little*, 1998], also confirmed by our field survey.

3. Depth Extent of Triggered Slip

To estimate the depth extent of the slip, we use models of elastic dislocations to invert surface displacement for the slip distribution [*Okada*, 1985]. While flexural-slip is related to the internal deformation of a fold, indicating the occurrence of plastic deformation, individual slip planes have been identified in field observations [*Townsend and Little*, 1998] and appear as localized discontinuities in Figure 2. Hence, we use elastic dislocation modeling to explain first-order surface signals resulting from the inferred flexural-slip displacement.

We solve for the best fitting slip distribution using a nonnegative least squares inversion [e.g., *Hamling et al.*, 2014, and references therein]. To enhance small signals associated with the triggered slip, we remove a modeled coseismic displacement of the *Mw* 6.6 Lake Grassmere earthquake [*Hamling et al.*, 2014] from the TerraSAR-X interferogram (Figures 4a and 4b). The surface traces of the inferred faults were found from the discontinuities in the LOS displacement. For modeling slip distributions, we do not deconvolve the deformation field into the horizontal and vertical components but directly use the LOS displacement field. The fault geometry is not solved for in the inversion procedure as the deformation signals associated with

©2015. American Geophysical Union. All Rights Reserved.

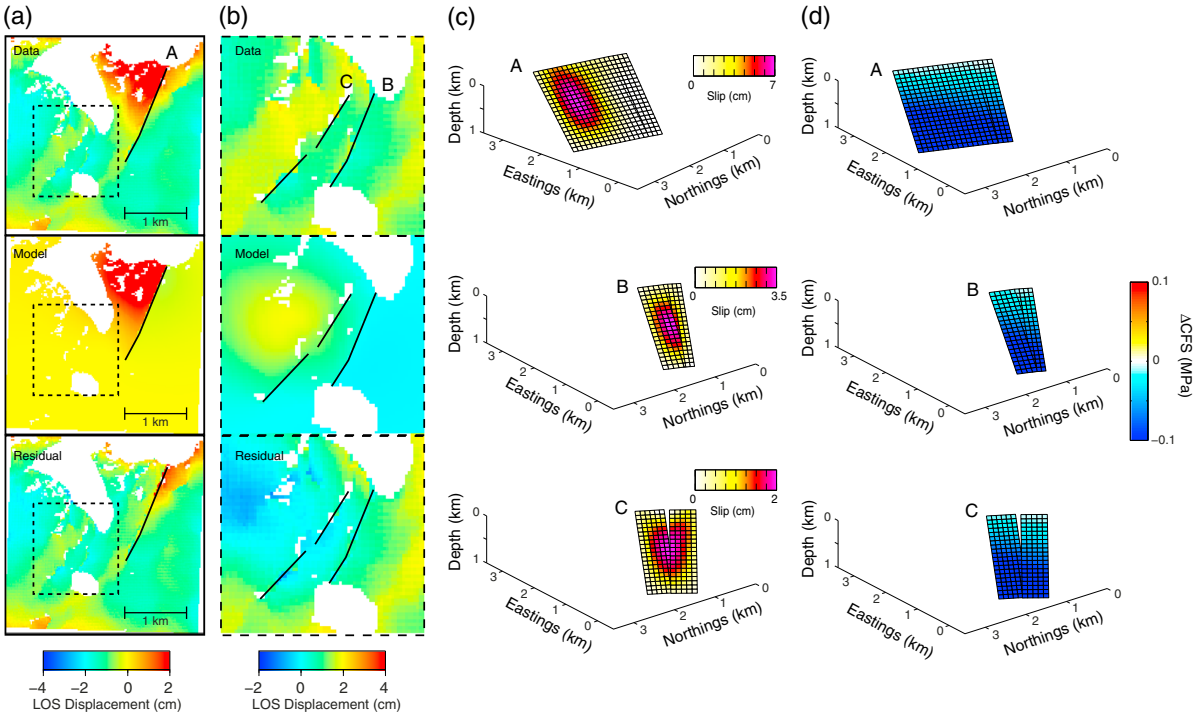

Figure 4. Line-of-sight (LOS) displacement from a TerraSAR-X interferogram, the best fitting LOS displacement from inverted slip distributions, and the residual for (a) the entire region and for (b) a subset (within a dashed box) that includes Faults B and C. The dip and rake angles are assumed to be 30° and 90° (i.e., pure dip slip), respectively. In Figure 4b, the LOS displacement is shifted by +1.4 cm uniformly to further remove the residual coseismic deformation by the main shock. (c) The inverted slip distributions on three flexural-slip faults. (d) Coulomb stress changes ΔCFS as a result of the *Mw* 6.6 Lake Grassmere earthquake resolved onto the fault planes where the triggered slip was imaged. Apparent friction coefficient $\mu' = 0.4$ is assumed.

the triggered slip are relatively small. Additionally, we find that the model does not fit to the data well for Faults B and C if the slip inversion is carried out for the entire area including all three faults (Figure 4a). Since surface deformation associated with Faults B and C is much smaller than that of Fault A, we perform separate slip inversion using a subset of the data containing Faults B and C (Figure 4b).

Figures 4a–4c show the best fitting LOS displacement and corresponding slip distributions on the three fault planes with an assumed dip angle of 30° and a rake of 90° (i.e., pure reverse dip slip). We choose the preferred slip models based on so-called L curve where the misfit starts to increase significantly while the model smoothness (i.e., the weight on the Laplacian of the slip distribution) increases only slightly (Figure S2). The preferred slip model indicates that up to 7 cm of dip slip had occurred on one of the fault planes and that slip on the other faults is smaller (up to ~3.5 cm). All the areas that experienced slip are confined within the top ~800 m, suggesting that the slip does not extend down to seismogenic depths (Figure 4c).

To determine parameter errors for our slip inversion, we follow a method of *Parsons et al.* [2006] and use a Monte Carlo simulation in which correlated noise, based on the 1-D covariance function ($C(r) = \sigma^2 e^{-\alpha r}$) to InSAR phase data away from the Lake Grassmere earthquake derived by *Hamling et al.* [2014] ($\sigma = 5.9$ mm, $\alpha = 1.8$ km), is used to perturb the data set 1000 times. For each of the new data sets, we solve for the best fitting slip distribution and obtain the distribution of values that provide an estimate of the uncertainty (Figure S3). Standard slip errors in the region of maximum slip is less than 1.2 cm, translating 17, 34, and 60% of the maximum slip on Faults A, B, and C, respectively. We also vary the assumed dip angle from 20° to 70°, which has little effect on the inverted slip distributions; the dominant slip in all the cases is still confined to shallow depths (< 1 km).

©2015. American Geophysical Union. All Rights Reserved.

4. Static or Dynamic Triggering

To assess if the triggered slip is more likely caused by static or dynamic stress changes, we calculate static Coulomb failure stress (ΔCFS) [e.g., *Stein et al.*, 1994; *King et al.*, 1994] on the fault planes using a slip model of the Lake Grassmere earthquake (Figure S4). Following the method of *Hamling et al.* [2010], we compute ΔCFS using the stress field projected onto the relevant fault planes and the apparent coefficient of friction μ', which include the effects of pore fluids and material properties in the fault zone [e.g., *Deng and Sykes*, 1997]. A positive ΔCFS implies that a fault is brought closer to failure, whereas a negative ΔCFS indicates that a fault is brought farther away from failure. We find that the ΔCFS is decreased by 0.05 MPa along all of the modeled fault planes, discouraging slip (Figure 4d). In Figure 4d, $\mu' = 0.4$ is assumed, but varying μ' from 0.2 to 0.8 does not alter the sign of ΔCFS (Figure S5). We also confirm that varying the assumed dip angle from 20° to 70° does not change the sign of ΔCFS.

Since the flexural-slip faults were brought farther away from failure by the static stress transfer and these shallow faults unlikely store enough elastic strain energy for the nucleation of seismic events, our results suggest that the observed shallow slip was not triggered by the static stress transfer but by the passage of seismic waves resulting from the *Mw* 6.6 Lake Grassmere earthquake. In this case, those flexural-slip faults would have been more stressed than others before the main shock. Similar inferences have been made for observed triggered surface slip in the Salton Trough region of southern California [e.g., *Williams et al.*, 1988; *Rymer*, 2000; *Wei et al.*, 2011].

5. Discussion

On 16 October 2013, 2 months after the *Mw* 6.6 Lake Grassmere earthquake, we searched for field evidence of the triggered slip near Lake Grassmere. While we found numerous small-scale (up to tens of meters) landslides at the sites of the inferred surface slip, we did not find any conclusive evidence of 1–2 cm fault slip extending ~1 km. Heavy rainfall events and vegetation growth during the 2 month period had likely obscured the ground surface signature of the relatively small slip that was imaged by two independent satellites.

Our results provide an important clue on how some slip on flexural-slip faults takes place. Although flexural-slip faults are not typically associated with large earthquakes, geological evidence suggests that slip along some flexural-slip faults is coseismic [*Yeats*, 1986]. For example, flexural-slip faulting has been documented or inferred during nearby earthquakes, including the 1981 M_L 2.5 Lompac earthquake (California) [*Yerkes et al.*, 1983], the 1980 *M* 7.3 El Asnam (Algeria) earthquake [*Philip and Meghraoui*, 1983], and the 1968 M 7.1 Inangahua earthquake (New Zealand) [*Lensen*, 1968; *Yeats*, 1986]. In all these cases, flexural-slip faults are thought to have moved in response to primary movement on bounding reverse faults (e.g., the London Hill fault in Figure 3) [*Yeats*, 1986]. However, the InSAR data did not show any evidence of slip on the London Hill fault (Figure 2). If slip on flexural-slip faults is triggered by the passage of seismic waves resulting from nearby large earthquakes, the slip could occur within a "coseismic" timescale as hinted by our observations. Our findings indicate that the movement of flexural-slip faults may involve transient stresses generated by the passage of seismic waves. Whether such triggering process applies to the movement of other flexural-slip faults remains a subject of future work.

For many large crustal earthquakes, the coseismic slip in the middle of the seismogenic layer is systematically larger than slip at the Earth surface [e.g., *Fialko et al.*, 2005; *Dolan and Haravitch*, 2014]. Since these seismic events were not associated with either resolvable shallow interseismic creep or robust shallow afterslip, there must be deficit of slip at shallow depths, which is eventually accommodated by other (off-fault) processes and/or greater shallow coseismic slip on neighboring active faults over time [*Kaneko et al.*, 2011; *Kaneko and Fialko*, 2011; *Dolan and Haravitch*, 2014]. Frequent occurrence of shallow triggered slip, caused by nearby large earthquakes, may provide an alternative explanation for such slip deficit at shallow depths if accumulated triggered slip is comparable to coseismic slip of a large earthquake in the middle of a seismogenic layer. Since the observed triggered slip is in a range of a few centimeters, such triggered slip must occur quite frequently in order for the shallow slip to be fully compensated. More studies and documentation of shallow triggered slip are needed to test this hypothesis.

©2015. American Geophysical Union. All Rights Reserved.

6. Conclusions

Using InSAR data, we have documented 1–2 cm of dip slip at the ground surface on three different northeast striking, northwest dipping, flexural-slip faults near the Lake Grassmere area in central New Zealand. These previously unmapped faults are located in the western limb of a syncline in the footwall of a known active reverse fault that did not move in the Lake Grassmere earthquake. The faults associated with the triggered slip are parallel to one another and separated by several hundred meters. The along-strike extent of the triggered slip is 1–1.5 km for each fault. Dislocation modeling of the InSAR data suggests that the triggered slip is confined to shallow depths. Coulomb stress analysis indicates that the slip was not triggered by the static stress change of the *Mw* 6.6 Lake Grassmere earthquake but was likely caused by dynamic shaking during the passage of seismic waves. Our findings suggest that the movement of some flexural-slip faults may involve transient stresses generated by the passage of seismic waves.

Acknowledgments

We thank Stephen Bannister for providing us the relocated seismicity catalog and Sigrún Hreinsdóttir for general discussion. Comments by anonymous reviewers helped us improve the manuscript. We also thank the Canadian Space Agency and German Aerospace Center (DLR) for access to RADARSAT-2 and TerraSAR-X data. This work was supported by public research funding from the Government of New Zealand. Computer codes used in the analysis have been cited in the Reference list and will be made available to anyone upon request.

The Editor thanks two anonymous reviewers for their assistance in evaluating this paper.

References

Costantini, M. (1998), A novel phase unwrapping method based on network programming, *IEEE Trans. Geosci. Remote Sens.*, *36*(3), 813–821.

Deng, J., and L. R. Sykes (1997), Evolution of the stress field in Southern California and triggering of moderate-size earthquakes: A 200-year perspective, *J. Geophys. Res.*, *102*, 9859–9886.

Dolan, J. F., and B. D. Haravitch (2014), How well do surface slip measurements track slip at depth in large strike-slip earthquakes? The importance of fault structural maturity in controlling on-fault slip versus off-fault surface deformation, *Earth Planet. Sci. Lett.*, *388*, 38–47.

Farr, T. G., et al. (2007), The shuttle radar topography mission, *Rev. Geophys.*, *45*, RG2004, doi:10.1029/2005RG000183.

Fialko, Y. (2004), Probing the mechanical properties of seismically active crust with space geodesy: Study of the co-seismic deformation due to the 1992 M_w7.3 Landers (southern California) earthquake, *J. Geophys. Res.*, *109*, B03307, doi:10.1029/2003JB002756.

Fialko, Y., D. Sandwell, M. Simons, and P. Rosen (2005), Three-dimensional deformation caused by the Bam, Iran, earthquake and the origin of shallow slip deficit, *Nature*, *435*, 295–299, doi:10.1038/nature03425.

Hamling, I. J., T. J. Wright, E. Calais, L. Bennati, and E. Lewi (2010), Stress transfer between thirteen successive dyke intrusions in Ethiopia, *Nat. Geosci.*, *3*, 713–717, doi:10.1038/ngeo967.

Hamling, I. J., E. D'Anastasio, L. M. Wallace, S. Ellis, M. Motagh, S. Samsonov, N. Palmer, and S. Hreinsdóttir (2014), Crustal deformation and stress transfer during a propagating earthquake sequence: The 2013 Cook Strait sequence, central New Zealand, *J. Geophys. Res. Solid Earth*, *119*, 6080–6092, doi:10.1002/2014JB011084.

Holden, C., A. Kaiser, R. V. Dissen, and R. Jury (2013), Sources, ground motion, and structural response characteristics in Wellington of the 2013 Cook Strait earthquakes, *Bull. N. Z. Soc. Earthquake Eng.*, *46*(4), 188–195.

Hudnut, K., L. Seeber, T. Rockwell, J. Goodmacher, R. Klinger, S. Lindvall, and R. McElwain (1989), Surface ruptures on cross-faults in the 24 November 1987 Superstition Hills, California, earthquake sequence, *Bull. Seismol. Soc. Am.*, *79*, 282–296.

Kaneko, Y., and Y. Fialko (2011), Shallow slip deficit due to large strike-slip earthquakes in dynamic rupture simulations with elasto-plastic off-fault response, *Geophys. J. Int.*, *186*, 1389–1403, doi:10.1111/j.1365-246X.2011.05117.x.

Kaneko, Y., J.-P. Ampuero, and N. Lapusta (2011), Spectral-element simulations of long-term fault slip: Effect of low-rigidity layers on earthquake-cycle dynamics, *J. Geophys. Res.*, *116*, B10313, doi:10.1029/2011JB008395.

King, G. C. P., R. S. Stein, and J. Lin (1994), Static stress changes and the triggering of earthquakes, *Bull. Seismol. Soc. Am.*, *84*, 935–953.

Lensen, G. J. (1968), Analysis of progressive fault displacement during downcutting at the Branch River terraces, South Island, New Zealand, *Geol. Soc. Am. Bull.*, *79*(5), 545–556.

Litchfield, N. J., et al. (2014), A model of active faulting in New Zealand, *N. Z. J. Geol. Geophys.*, *57*(1), 32–56.

Okada, Y. (1985), Surface deformation due to shear and tensile faults in a half-space, *Bull. Seismol. Soc. Am.*, *75*, 1135–1154.

Parsons, B., T. Wright, P. Rowe, J. Andrews, J. Jackson, R. Walker, M. Khatib, M. Talebian, E. Bergman, and E. R. Engdahl (2006), Sefidabeh (eastern Iran) earthquakes revisited: New evidence from satellite radar interferometry and carbonate dating about the growth of an active fold above a blind thrust fault, *Geophys. J. Int.*, *164*(1), 202–217, doi:10.1111/j.1365-246X.2005.02655.x.

Philip, H., and M. Meghraoui (1983), Structural analysis and interpretation of the surface deformations of the El Asnam earthquake of October 10, 1980, *Tectonics*, *2*(1), 17–49.

Pondard, N., and P. M. Barnes (2010), Structure and paleoearthquake records of active submarine faults, Cook Strait, New Zealand: Implications for fault interactions, stress loading, and seismic hazard, *J. Geophys. Res.*, *115*, B12320, doi:10.1029/2010JB007781.

Rattenbury, M. S., D. B. Townsend, and M. R. Johnston (2000), Geology of the Kaikoura area, *Tech. rep.*, GNS Science, Lower Hutt, New Zealand, institute of Geological and Nuclear Sciences 1:250,000 geological map 13, 1 sheet + 70 p.

Rymer, M. J. (2000), Triggered surface slips in the Coachella Valley area associated with the 1992 Joshua Tree and Landers, California, earthquakes, *Bull. Seismol. Soc. Am.*, *90*, 832–848.

Stein, R., G. King, and J. Lin (1994), Stress triggering of the 1994 M = 6.7 Northridge, California, earthquake by its predecessors, *Science*, *265*, 1432–1435.

Townsend, D. B., and T. A. Little (1998), Pliocene-Quaternary deformation and mechanisms of near-surface strain close to the eastern tip of the Clarence Fault, northeast Marlborough, New Zealand, *N. Z. J. Geol. Geophys.*, *41*, 401–417, doi:10.1080/00288306.1998.9514819.

Van Dissen, R., et al. (2013), Landslides and liquefaction generated by the Cook Strait and Lake Grassmere earthquakes: A reconnaissance report, *Bull. N. Z. Soc. Earthquake Eng.*, *46*(4), 196–200.

Wallace, L. M., P. Barnes, J. Beavan, R. Van Dissen, N. Litchfield, J. Mountjoy, R. Langridge, G. Lamarche, and N. Pondard (2012), The kinematics of a transition from subduction to strike-slip: An example from the central New Zealand plate boundary, *J. Geophys. Res.*, *117*, B02405, doi:10.1029/2011JB008640.

Wegmüller, U., and C. Werner (1997), Gamma SAR processor and interferometry software, in *Proceedings of the 3rd Symposium on Space at the Service of Our Environment, Florence, Italy*, pp. 1687–1692, (ESA SP-414), Estec, Noordwijk, Netherlands.

Wei, M., D. Sandwell, Y. Fialko, and R. Bilham (2011), Slip on faults in the Imperial Valley triggered by the 4 April 2010 *Mw* 7.2 El Mayor-Cucapah earthquake revealed by InSAR, *Geophys. Res. Lett.*, *38*, L01308, doi:10.1029/2010GL045235.

©2015. American Geophysical Union. All Rights Reserved.

Williams, P. L., S. F. McGill, K. E. Sieh, C. R. Allen, and J. N. Louie (1988), Triggered slip along the San Andreas fault after the 8 July 1986 North Palm Springs earthquake, *Bull. Seismol. Soc. Am.*, *78*, 1112–1122.
Wright, T., B. Parsons, and Z. Lu (2004), Toward mapping surface deformation in three dimensions using InSAR, *Geophys. Res. Lett.*, *31*, L01607, doi:10.1029/2003GL018827.
Yeats, R. S. (1986), Active faults related to folding, in *Active Tectonics*, pp. 63–79, National Acad. Press, Washington, D. C.
Yerkes, R. F., W. L. Ellsworth, and J. C. Tinsley (1983), Triggered reverse fault and earthquake due to crustal unloading, northwest Transverse Ranges, California, *Geology*, *11*(5), 287–291.

©2015. American Geophysical Union. All Rights Reserved.

Supplementary Material for article "InSAR imaging of displacement on flexural-slip faults triggered by the 2013 Mw 6.6 Lake Grassmere earthquake, central New Zealand"

Y. Kaneko,[1] I. J. Hamling,[1] R. J. Van Dissen,[1]

M. Motagh[2], and S. V. Samsonov[3]

Corresponding author: Y. Kaneko, GNS Science, 1 Fairway Drive, Avalon, Lower Hutt, New Zealand. (y.kaneko@gns.cri.nz)

[1]GNS Science, Lower Hutt, New Zealand

[2]GFZ German Research Centre for Geosciences, Potsdam, Germany

[3]Natural Resources Canada, Ottawa, Ontario, Canada

References

Eberhart-Phillips, D., M. Reyners, S. Bannister, M. Chadwick, and S. Ellis, Establishing a versatile 3-D seismic velocity model for New Zealand, *Seismol. Res. Lett.*, *81*(6), 992–1000, 2010.

Hamling, I. J., E. D'Anastasio, L. M. Wallace, S. Ellis, M. Motagh, S. Samsonov, N. Palmer, and S. Hreinsdóttir, Crustal deformation and stress transfer during a propagating earthquake sequence: The 2013 Cook Strait sequence, central New Zealand, *J. Geophys. Res.*, *119*, 6080–6092, doi:10.1002/2014JB011084, 2014.

Parsons, B., T. Wright, P. Rowe, J. Andrews, J. Jackson, R. Walker, M. Khatib, M. Talebian, E. Bergman, and E. R. Engdahl, The 1994 Sefidabeh (eastern Iran) earthquakes revisited: new evidence from satellite radar interferometry and carbonate dating about the growth of an active fold above a blind thrust fault, *Geophys. J. Int.*, *164*(1), 202–217, doi:10.1111/j.1365-246X.2005.02655.x, 2006.

Waldhauser, F., HypoDD: A computer program to compute double-difference earthquake locations, USGS Open File Rep., 01-113, 2001.

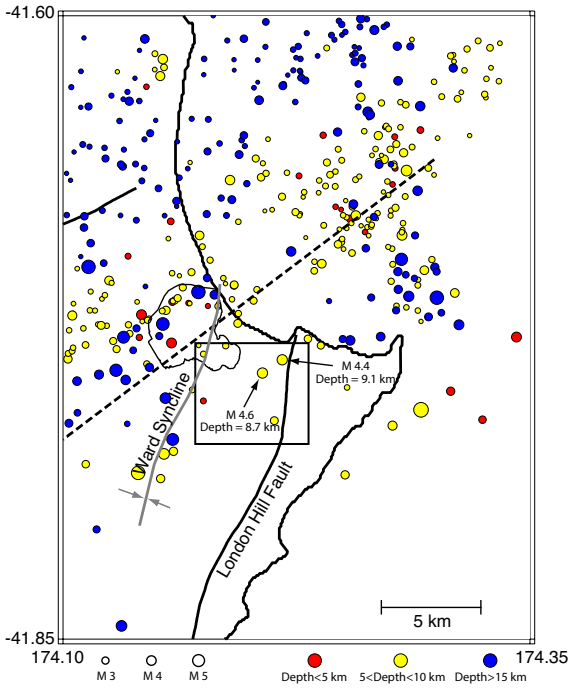

Supplementary Figure 1. Relocated seismicity around the Lake Grassmere region during 20 – 25 August, 2013. Earthquake relocations were carried out using the hypodd3D (version 2.0b) software of *Waldhauser* [2001], with the 3-D New Zealand velocity model of *Eberhart-Phillips et al.* [2010]. There are two ∼M4 aftershocks near the sites of triggered slip but surface rupture of these moderate events were unlikely given their deep hypocenters (∼9 km).

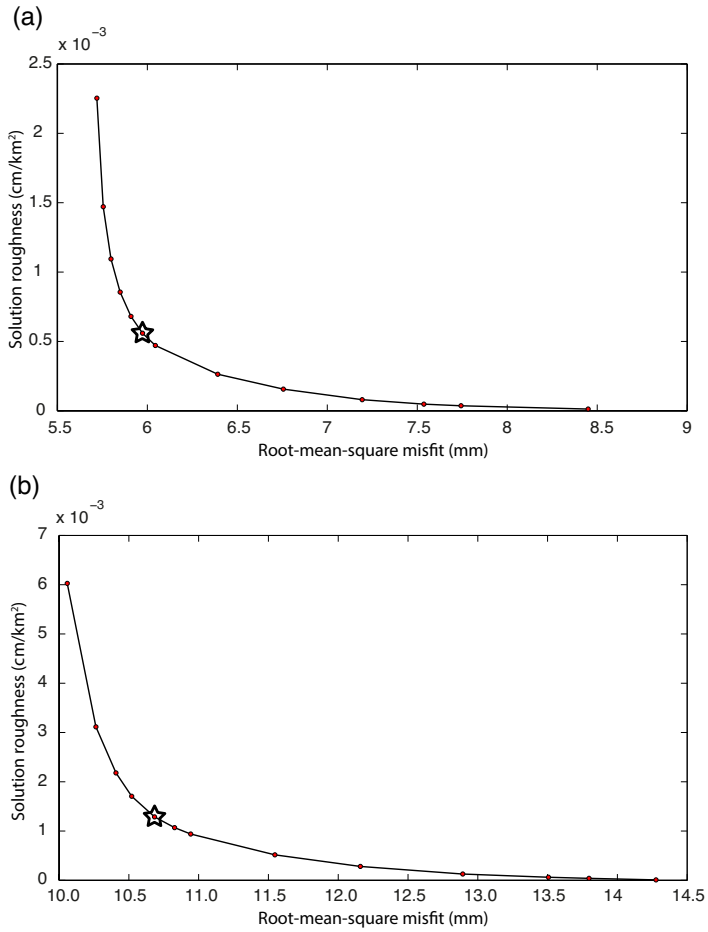

Supplementary Figure 2. L-curve smoothing plots for the slip distribution on (a) Fault A and (b) Faults B and C shown in Figure 4. The star indicates the chosen solutions shown in Figure 4c.

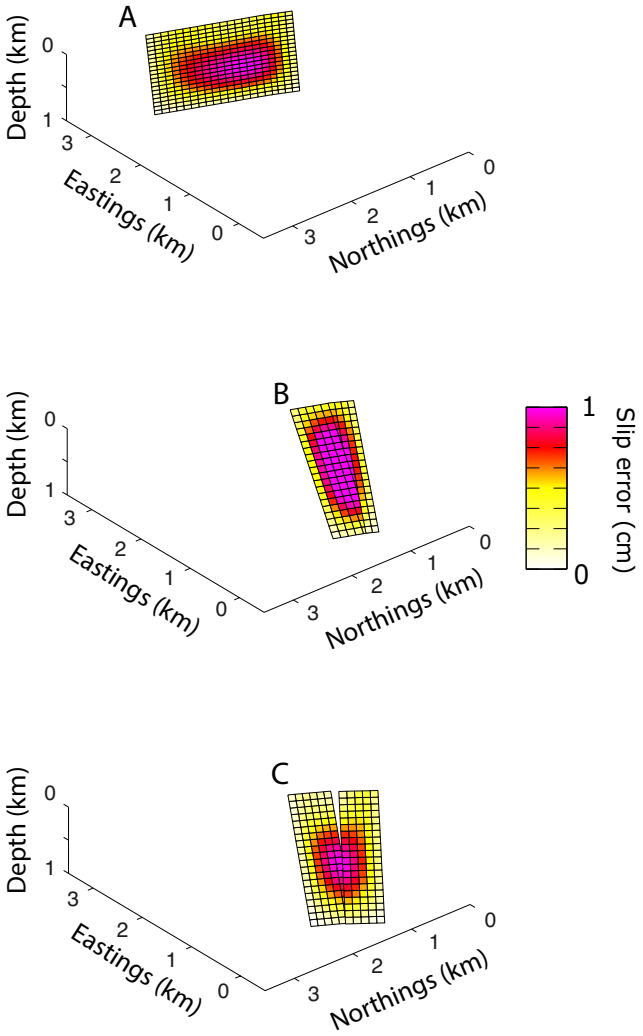

Supplementary Figure 3. Standard deviation of slip errors on three fault planes shown in Figure 4c. Slip errors are calculated by a Monte-Carlo simulation in which correlated noise, based on the 1-D covariance function ($C(r) = \sigma^2 e^{-\alpha r}$) to phase data away from the Lake Grassmere earthquake derived by *Hamling et al.* [2014] ($\sigma = 5.9$ mm, $\alpha = 1.8$ km), is used to perturb the dataset 1000 times [e.g. *Parsons et al.*, 2006]. The slip errors are less than 1.2 cm on all the fault planes.

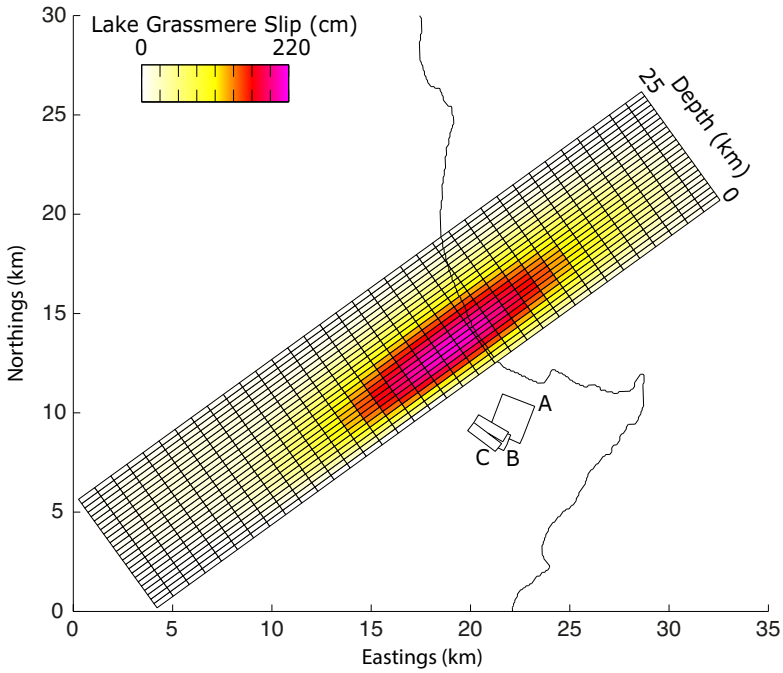

Supplementary Figure 4. Map showing the slip model of the 2013 Mw 6.6 Lake Grassmere earthquake [*Hamling et al.*, 2014] and the locations of the three faults associated with surface slip imaged by the InSAR data. The geodetic solution indicates that the fault associated with the mainshock has a dip and rake of 70° and 168°, respectively.

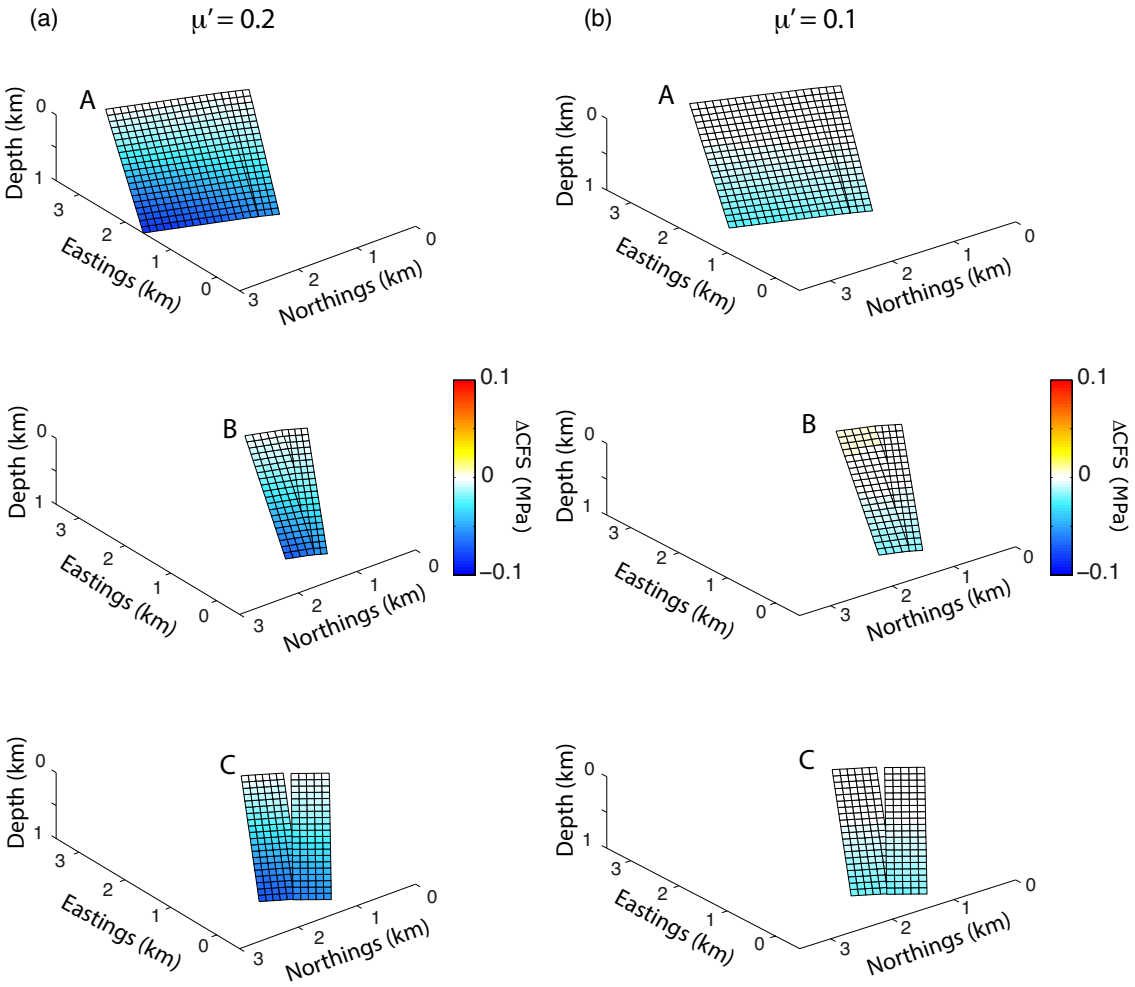

Supplementary Figure 5. Coulomb stress changes ΔCFS as a result of the Mw 6.6 Lake Grassmere earthquake resolved onto the fault planes where the triggered slip was imaged. Cases with assumed apparent friction coefficient (a) $\mu' = 0.2$ and (b) $\mu' = 0.1$ are shown. The amplitude of the ΔCFS depends on μ' while the sign of ΔCFS is systematically negative for all the cases with $\mu' \geq 0.2$. ΔCFS is an order of magnitude smaller for $\mu' = 0.1$ than $\mu' = 0.4$.